Journal of Contaminant Hydrology 226 (2019) 103518

Contents lists available at ScienceDirect

Journal of Contaminant Hydrology

journal homepage: www.elsevier.com/locate/jconhyd

Climate change impact on residual contaminants under sustainable remediation

Arianna Libera[a,*], Felipe P.J. de Barros[a], Boris Faybishenko[b], Carol Eddy-Dilek[c], Miles Denham[d], Konstantin Lipnikov[e], David Moulton[e], Barbara Maco[f], Haruko Wainwright[b]

[a] Sonny Astani Dept. of Civil and Environmental Engineering, University of Southern California, Los Angeles, California, USA
[b] Lawrence Berkeley National Laboratory, Berkeley, CA, USA
[c] Savannah River National Laboratory, Aiken, SC, USA
[d] Panoramic Environmental Consulting, LLC, Aiken, SC, USA
[e] Los Alamos National Laboratory, Los Alamos, NM, USA
[f] Wactor & Wick LLP Environmental Lawyers, Oakland, CA, USA

ABSTRACT

This study investigates the potential impact of climate change on residual contaminants in vadose zones and groundwater. We assume that the effect of climate changes can be represented by perturbations in the natural recharge through the aquifer system. We perform numerical modeling of unsaturated/saturated flow and transport and consider different performance metrics: contaminant concentrations at observation wells and contaminant export at the site's boundary. We evaluate the effect of increasing and decreasing recharge as well as the impact of potential failure of surface capping structures employed to immobilize vadose zone contaminants. Our approach is demonstrated in a real case study by simulating transport of non-reactive radioactive tritium at the U.S. Department of Energy's Savannah River Site. Results show that recharge changes significantly affect well concentrations: after an initial slight dilution we identify a significant concentration increase at different observation wells some years after the recharge increase and/or the cap failure, as a consequence of contaminants' mobilization. This effect is generally emphasized and occurs earlier as the recharge increases. Under decreased aquifers' recharge the concentration could slightly increase for some years, due to a decrease of dilution, depending on the magnitude of the negative recharge shift. We identify trigger levels of recharge above which the concentration/export breakthrough curves and the time of exceedance of the Maximum Contaminant Level for tritium are remarkably affected. Moreover, we observe that the contaminant export at the control plane, identified as the risk pathway to the downgradient population, may only be minimally affected by shifts in the natural recharge regime, except for some extreme cases. We conclude that more frequent sampling and in-situ monitoring near the source zone should be adopted to better explain concentrations' anomalies under changing climatic conditions. Moreover, the maintenance of the cap is critical not only to sequester residual contaminants in the vadose zone, but also to reduce the uncertainty associated with future precipitation changes. Finally, realistic flow and transport simulations achieved through proper calibration processes, rather than conservative modeling, should be adopted to identify non-trivial trade-offs which enable better allocation of resources towards reducing uncertainty in decision making.

1. Introduction

Subsurface contamination is recognized as a critical issue in many communities. There are more than a thousand Superfund sites in the U.S. categorized under the U.S. Environmental Protection Agency (EPA), which present large plumes of organic solvents, heavy metals and radionuclides (US Environmental Protection Agency, https://www.epa.gov/superfund). In addition, the EPA estimated the presence of more than 450,000 brownfields in the U.S., contaminated by hazardous substances, pollutants or contaminants (US Environmental Protection Agency, https://www.epa.gov/brownfields).

The practice of soil and groundwater remediation has been changing in recent decades, transitioning from intense soil removal and active treatment solutions towards passive remediation techniques such as enhanced biodegradation or monitored natural attenuation (Ellis and Hadley, 2009). The latter less-intensive remediation approaches, often identified as *sustainable remediation* techniques, have been recognized as more advantageous since they can reduce negative side effects that often accompany intensive remediation (e.g., ecological disturbance, construction noise/traffic, intensive energy use and emissions of greenhouse gases). Additionally, sustainable remediation is coupled with more innovative and attractive end-use scenarios with restricted subsurface use and longer institutional control. In most cases, a portion of contaminants are sequestered in the subsurface for a long period of time, while natural or enhanced biogeochemical processes occur to reduce contaminant concentrations. Within this context, it is critical to assess the long-term stability of residual contaminants subject to sustainable remediation practices and to ensure that the latter will not pose

* Corresponding author.
E-mail address: libera@usc.edu (A. Libera).

https://doi.org/10.1016/j.jconhyd.2019.103518
Received 22 March 2019; Received in revised form 17 June 2019; Accepted 25 June 2019
Available online 27 June 2019
0169-7722/

significant environmental and human health risk.

Recently, O'Connell and Hou (2015a) raised the concern that climate change may pose a major risk in environmental remediation; especially with regard to the fate of residual contaminants under sustainable remediation. A hydrological shift has been identified as one of the key drivers influencing such risk and uncertainty. In changing climate, precipitation regimes (including amount and timing) are expected to change significantly, and extreme events, such as heavy rains and prolonged droughts, could become more frequent. Climate models also predict increasing temperatures, which would affect water budgets and reduce infiltration due to increased evapotranspiration. These climatic changes are occurring while groundwater is becoming increasingly important for drinking and irrigation purposes (Famiglietti, 2014).

Despite the critical need to evaluate risks associated with climate change, there is only a limited number of studies that address the effects of climate change on contaminant transport and environmental remediation. While the impact of climate change has been investigated extensively from the perspective of water resources (Gellens and Roulin, 1998; Green et al., 2011; Middelkoop et al., 2001; Pfister et al., 2004), a limited number of studies have addressed water quality issues (Visser et al., 2012). Moreover, most literature focuses on surface water (Wilby et al., 2006; Van Vliet and Zwolsman, 2008; Van Bokhoven, 2006; Futter et al., 2009; Schiedek et al., 2007), due to its visibility and accessibility (Green et al., 2011), while the studies on groundwater are mostly focused on agricultural effluents at the regional scale (Bloomfield et al., 2006; Futter et al., 2009; Li and Merchant, 2013; Olesen et al., 2007; Sjoeng et al., 2009; Whitehead et al., 2009; Wilby et al., 2006; Darracq et al., 2005; Destouni and Darracq, 2009; Park et al., 2010). Current literature lacks site-scale hydrological studies that can guide sustainable remediation under changing climate conditions within risk and performance assessments as well as within regulatory frameworks.

This study aims at evaluating the effects of climate-driven hydrological shifts on residual contaminants in vadose zones and groundwater under sustainable remediation. We simulate groundwater flow and contaminant transport through unsaturated and saturated domains. We assume that the effect of changing precipitation and temperature can be represented by perturbations/shifts of natural recharge through the aquifer system. The impacts are evaluated on the basis of different decision metrics relevant to public health risk, regulatory compliance and site closure such as contaminant concentrations at monitoring wells and exports from site boundaries. We demonstrate our approach at the Department of Energy (DOE)'s Savannah River Site (SRS) F-Area Seepage Basins, South Carolina (SC), USA, where soil and groundwater were contaminated by various metals and radioactive contaminants during the Cold War Era. For brevity, the F-Area Seepage Basins are referred to hereafter as just F-Area. Extensive subsurface characterization and dataset at the SRS F-Area, including hundreds of wells, geophysics data and various hydrological tests, enabled the development of a subsurface model that can be considered as a testbed for flow and transport studies (Flach, 2004; Bea et al., 2013; Sassen et al., 2012; Wainwright et al., 2014; Dai et al., 2002). The SRS hence provides a unique opportunity to investigate the potential consequences of climate change on residual contamination in realistic settings that display multiple representative features of other polluted sites.

2. Background

2.1. Conceptual model

We consider a general conceptual hydrological model of a contaminated site characterized by residual contamination in the vadose zone and groundwater (Fig. 1). This model extends to the SRS F-Area (Bea et al., 2013), the description of which is provided in Section 2.2. Initially, contaminants are discharged through a seepage basin located on the top of the model domain. The contaminant plume migrates vertically through the vadose zone, and laterally downgradient in the aquifer. At some sites, the plume reaches surface water bodies (e.g., a creek or a river) located close to the site boundary, through water seepage. In order to reduce contaminant migration through the vadose zone, the contaminant source zone (i.e., seepage basin) is often capped with low-permeability material, such as clay or silt. However, residual contaminants located in the vadose zone could become a persistent contaminant source to the groundwater plume (Zachara et al., 2013), as shown in Fig. 1.

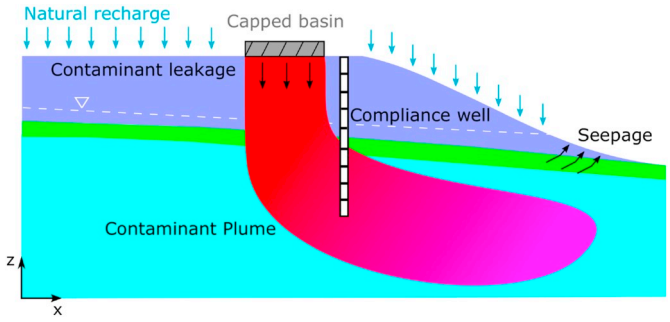

Fig. 1. Schematic illustration of the hydrological conceptual model under investigation, representing a vertical two-dimensional cross-section driven along the middle line of the contaminant source zone.

Contaminant concentrations are typically measured at groundwater monitoring wells to ensure the plume stability and to meet the regulatory compliance. The number of wells and frequency of sampling (e.g., quarterly or annually) are determined in agreement with a regulatory agency (e.g., the EPA). Concentrations are often compared to the Maximum Contaminant Level (MCL) recommended by the EPA. Predicting the time of exceedance of MCL, for example, is an important Environmental Performance Metric (EPM) to plan the site closure or site transfer (Denham and Eddy-Dilek, 2017). In parallel, risk (and/or performance) assessments consider a variety of metrics and pathways, including contaminant mass flux/export at control planes (CPs), e.g., site boundaries, creeks or rivers (Maxwell and Kastenberg, 1999; de Barros and Rubin, 2008; de Barros et al., 2009, 2012; Atchley et al., 2013). On-site concentrations are often used to evaluate human health risk doses through direct ingestion/drinking pathways, while the export at CPs are employed to quantify risk of the downgradient population.

The changes in precipitation and temperature associated with climate change are expected to affect contaminant plumes in groundwater systems and residual contaminants in the vadose zone in a complex manner. This impact can be evaluated by considering a perturbation/shift of the natural recharge through an aquifer in a long or short time frame (O'Connell and Hou, 2015b). For example, an increase in precipitation results in higher aquifer recharge, while a decrease in precipitation, or higher temperature, hence increased evapotranspiration, leads to lower aquifer recharge. Higher recharge then (1) increases vadose-zone flow, which mobilizes sequestered contaminants, (2) raises the groundwater table and increases hydraulic gradients, resulting in enhanced plume mobility in groundwater, and (3) enhances mixing of the plume with clean water, which leads to higher dilution. On the other hand, a decrease of recharge has opposite effects, i.e., decreases the plume mobility while reducing mixing and dilution. The impact of climate change-driven altered recharge rates on different decision and performance metrics relevant to environmental remediation could potentially create trade-offs that should be quantitatively evaluated.

2.2. F-Area site description

The SRS is located in South-central South Carolina, USA, approximately 100 mi (i.e., 161 km) away from the Atlantic Ocean and occupies an area of about 800 km^2. The site was used to produce nuclear

materials such as plutonium and tritium (^{3}H), for nuclear weapons during the Cold War Era. The F-Area, located in the north-central part of the SRS, included three unlined discharge basins: F-1, F-2 and F-3 (Bea et al., 2013). The basins received approximately 7.1 billion liters of acidic, low-level radioactive waste solutions from processing irradiated uranium between 1955 and 1988 (Flach et al., 2004; Killian et al., 1986). The waste solution presented various radionuclides such as uranium isotopes, ^{90}Sr, ^{129}I and ^{99}Tc, among which ^{3}H, is the largest dose contributor. After the waste discharge operation was terminated in 1988, the F-Area basins were closed and capped with low-permeability material (Bea et al., 2013). Currently, an acidic contaminant plume extends from the basins approximately 600 m downgradient to the groundwater seepage near the Fourmile Branch (Bea et al., 2013). Enhanced natural attenuation is currently under way using a funnel-and-gate system which consists of groundwater flow barriers to decrease the groundwater gradient, and base injection to neutralize pH and to immobilize uranium (Tokunaga et al., 2012).

Hydrogeology at this site has been characterized extensively in many studies (Flach et al., 2004; Bea et al., 2013; Sassen et al., 2012; Wainwright et al., 2014). There are three hydrostratigraphic units within the Upper Three Runs Aquifer: an Upper Aquifer zone (UUTRA), a Tan Clay Confining Zone (TCCZ), and a Lower Aquifer zone (LUTRA). The UUTRA and LUTRA are mainly composed by clean sand, while the TCCZ is a low-permeable mixed sand-and-clay layer. The piezometric head measurements indicate that the UUTRA and LUTRA units are hydrologically connected. The bottom of the LUTRA consists of a competent clay layer confining unit, the continuous Gordon Confining (GC) unit, which separates the deeper aquifer (Gordon Aquifer) from the upper two units. The historical monitoring data collected at the SRS have shown that the contaminant plume migrates within the UUTRA and LUTRA (Sassen et al., 2012).

3. Methodology

3.1. Flow and transport simulations

We employ the two-dimensional (2D) flow and transport model adopted in Bea et al. (2013), i.e., a 2D domain approximately 2600 m long and 100 m deep along the groundwater flow line, passing through the middle of the F-3 basin of the SRS. This model has been calibrated and verified using site data (Bea et al., 2013). Fig. 2 illustrates the 2D cross-section model domain.

The model includes the vadose zone and three hydrostratigraphic units (i.e., UUTRA, LUTRA and TCCZ) defined in Section 2.2. We assume homogeneous average hydrogeological properties within each unit (see Table 1), whose values are compiled from available site investigation reports. Table 1 specifies porosity, permeability and capillary pressure/saturation data for the vadose zone (Flach et al., 2004; Phifer et al., 2006; Bea et al., 2013). Please refer to Appendix A of Bea et al. (2013) for the parameters description. The system is considered to be advective dominated, therefore mechanical dispersion and molecular diffusion transport processes are neglected. We simulate simple ^{3}H decay with a half-life of 12.3 years. No-flow boundary conditions are assigned along the two vertical sides of the 2D-cross section (see Fig. 2) according to the groundwater divides (Flach, 2004; Bea et al., 2013). An impervious flow boundary condition (i.e. no-flow) is set at the bottom of the computational domain, since the confining unit at this location is highly clayey and continuous (Bea et al., 2013).

Groundwater flow and contaminant transport are simulated by means of the numerical code Amanzi which describes coupled vadose zone and groundwater flow as well as reactive transport (Freshley et al., 2012; Bea et al., 2013; Wainwright et al., 2015, 2016). Amanzi uses the mimetic finite difference method for the Richards equation and dispersion operators, which preserves fundamental mathematical and physical properties in discrete schemes (da Veiga et al., 2014). To discretize the advection operator, it uses monotone first-order and second-order MUSCL schemes with new limiters that improve accuracy on unstructured meshes (Lipnikov et al., 2010). Amanzi has been benchmarked against other flow and transport models as well as analytical solutions for a wide range of hydrological problems.

We perform numerical simulations within the time frame 1955–2100, i.e., from the beginning of the discharge operation at the SRS. Our model is discretized into 164,160 cells and we adopt a longitudinal mesh spatial resolution of 1.25 m and a variable vertical spatial resolution, with a maximum value of 2 m. A steady-state simulation is carried out to establish the groundwater table with a given recharge value at the top of the modeled domain of 4.74×10^{-6} mm/s (i.e., 150 mm/yr) before 1955. This value represents the estimated recharge

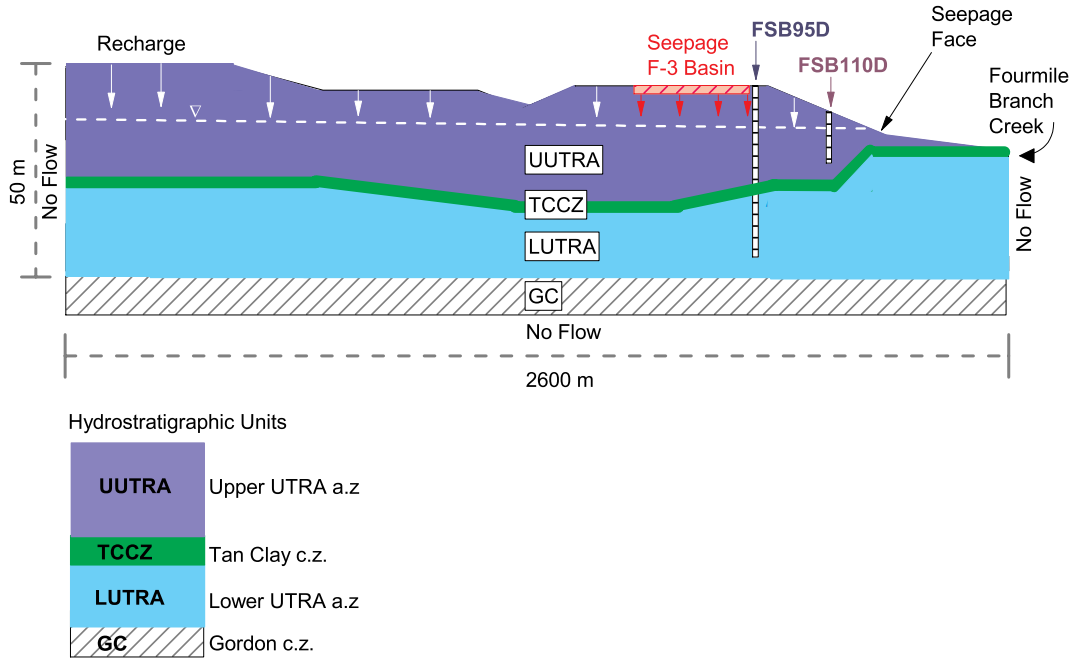

Fig. 2. Two-dimensional model domain adopted in our study.

Table 1
Parameters adopted in the numerical model presented in this study. The table reports values for porosity (ϕ [−]), permeability (k [m^2]), water retention-curve parameters (α [kg^{-1} m s^2], n [−], m [−]), residual liquid pore saturation (S_H [−]), Mualem (1976) parameter (p [−]) (for details, see Bea et al., 2013).

Hydrostratigraphic Unit	Porosity ϕ [−]	Permeability k [m^2]	α [kg^{-1} m s^2]	n [−]	m [−]	S_H [−]	p [−]
UUTRA	0.39	5×10^{-12}	4×10^{-4}	2	0.5	0.18	1
TCCZ	0.39	1.98×10^{-14}	5.1×10^{-5}	2	0.5	0.39	1
LUTRA	0.39	5×10^{-12}	5.1×10^{-5}	2	0.5	0.41	1

based on the rainfall records and runoff estimations (Flach et al., 2004), which is kept constant over the entire domain for all the simulation timeframe, except for the discharge basin. After 1955, we perform transient simulations employing a constant ^{3}H discharge value at the seepage basin between 1955 and 1988. The average ^{3}H concentration and mass discharge rate are respectively 2.17×10^{-9} mol/kgw and around 1.11×10^{-4} mm/s, as in Bea et al. (2013). These values coincide with the average ^{3}H concentration and discharge rate of historical data between 1955 and 1988 (see Table 8 of Bea et al. (2013)). After the basin is capped in 1988, the recharge through the basin is assumed to be three-order of magnitude lower than the value of the surrounding regions for all the simulations performed in our study. These recharge values are identified as baseline recharge conditions in our study.

We model different recharge scenarios which present increased or decreased recharge values with respect to the baseline recharge conditions described above. We analyze the impact of recharge shifts on different decision (or performance) metrics: the temporal evolution of ^{3}H concentration at the same two observation wells of Bea et al. (2013), shown in Fig. 2: (1) the source-zone UUTRA well (FSB95D) and (2) the downgradient UUTRA well (FSB110D). Both wells span the upper aquifer. Please note that we computed the contaminant concentration by taking the average value of the concentration reported at a set of observation points equally spaced within a given well in the upper aquifer. In addition, we evaluate the ^{3}H export at the CP to the Fourmile Branch Creek (see Fig. 2), which is the main risk pathway at this site. The CP is defined at the seepage face (indicated in Fig. 2) where the groundwater flow reaches the surface. The concentrations are compared with the EPA's MCL for ^{3}H. Although the MCL criteria is not used for compliance purposes at the SRS, it has been used to evaluate the timeframe for the site closure and transfer (Denham and Eddy-Dilek, 2017).

3.2. Modeling scenarios

Previous studies on the SRS have reported an overall trend towards greater rainfall in the region (Faybishenko et al., 2018). According to the National Climate Assessment, South Carolina is expected to see precipitation increases of 10%–20% by 2100 (see Fig. 7.5 in Easterling et al. (2017)), as well as more extreme precipitation event by up to two-folds (see Fig. 7.6 in Easterling et al. (2017)). Even if the amount of precipitation is not necessarily equal to the recharge, we assume that we can investigate the impact of climate change by simulating a range of different recharge values. The range would also account for the uncertainty associated with the climate projections. We mainly focus on increased natural recharge conditions, although, for completeness, we also investigate the impact of reduced recharge. Fig. 3 provides an illustration of the recharge scenarios simulated in our analysis. We consider a baseline recharge, denoted as R_B, and indicated by the black line in Fig. 3. To study the effect of climate change-induced increased/decreased recharge on contaminant transport, we define ϵ to be a perturbation from the baseline recharge and R_P to identify the perturbed recharge. We develop four perturbed recharge scenarios with respect to the baseline recharge conditions, corresponding to $\epsilon = 0$, described in the Section 3.1. The recharge perturbation starts at a certain time, set to year 2020, and is illustrated with a specific colour for each scenario in Fig. 3. In the following, we provide a detailed

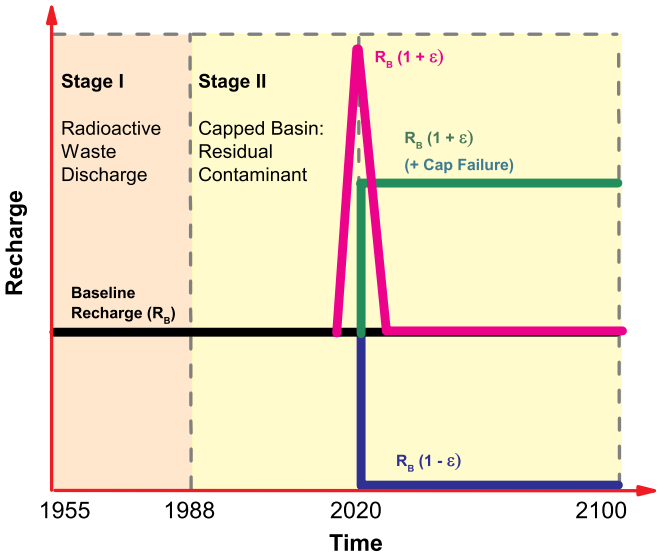

Fig. 3. Schematic illustration of the perturbed recharge scenarios analyzed in the study: (1) the constant positive recharge shift starting in 2020 (green line), (2) the constant negative recharge shift starting in 2020 (blue line), (3) the one-year extreme recharge in 2020 (magenta line) and (4) the hypothetical cap failure and constant positive recharge shift starting in 2020 (green line). The baseline recharge scenario is denoted by the horizontal black line. (For interpretation of the references to colour in this figure legend, the reader is referred to the web version of this article.)

description of the scenarios and of the values adopted for ϵ and we employ t^* to indicate year 2020.

3.2.1. Constant positive recharge shift

The recharge conditions of the first scenario (portrayed in green, from year 2020, in Fig. 3) are illustrated through the following equation:

$$R_P(t) = \begin{cases} R_B, & if \quad t < t^* \\ R_B(1 + \epsilon), & if \quad t \geq t^* \end{cases} \tag{1}$$

through this scenario we simulate a constant positive shift (i.e., an increase) of recharge from 2020 until the end of the simulation, set to year 2100. The perturbation ϵ assumes the following range of values: $\epsilon = [0.1, 0.2, 0.3, 0.4, 0.5]$, we therefore simulate a recharge increase of +10% to +50% compared to baseline recharge conditions.

3.2.2. Constant negative recharge shift

By the same token, the second scenario (blue line from year 2020 in Fig. 3) is illustarted through the following equation:

$$R_P(t) = \begin{cases} R_B, & if \quad t < t^* \\ R_B(1 - \epsilon), & if \quad t \geq t^* \end{cases} \tag{2}$$

this scenario is characterized by a constant negative shift of recharge (i.e., a decrease) of −10% to −50% ($\epsilon = [0.1, 0.2, 0.3, 0.4, 0.5]$ from Eq. (2)) within the timeframe 2020–2100.

3.2.3. One-year extreme recharge

The third scenario (magenta line from 2020 in Fig. 3) is described by:

$$R_P(t) = \begin{cases} R_B, & if \quad t < t^* \\ R_B(1+\epsilon), & if \quad t^* \le t \le t^*+1 \end{cases} \tag{3}$$

this scenario considers a significant increase of recharge within year 2020, mimicking an extreme precipitation event of a factor of 1.5, 2, 5 and 10 folds compared to baseline conditions. The range of perturbation values of this third scenario, according to Eq. (3), are then: $\epsilon =$ [0.5, 1, 4, 9].

3.2.4. Cap failure and constant positive recharge shift

The cap failure is also evaluated in conjunction with the natural recharge shift. Although low-permeability material is used for capping the F-Area basins, increased vegetation or other mechanisms could threaten the integrity of the source-zone capping structure (Worthy et al., 2013a, 2013b, 2015). In the fourth scenario, we assume that the cap will fail at the same time of the recharge increase (i.e., in year 2020). Note that the assumption of cap failure in 2020 is solely for the purpose of the modeling exercise and not a prediction of actual cap failure. The perturbed recharge conditions of this scenario are then the same of the first scenario, i.e.:

$$R_P(t) = \begin{cases} R_B, & if \quad t < t^* \\ R_B(1+\epsilon), & if \quad t \ge t^* \end{cases} \tag{4}$$

The cap failure is represented by increased source-zone recharge to the level of the surrounding region, therefore we hypothesize a complete failure of the containment structure. Although such a sudden failure is unlikely to happen, we assume instant failure to evaluate the most extreme case. The fourth scenario simulates the failure of the capping structure in arbitrarily assumed year 2020 under baseline recharge conditions and under the increased recharge conditions of the first scenario, characterized by $\epsilon =$ [0.1, 0.2, 0.3, 0.4, 0.5], from 2020 to 2100.

In reality, such precipitation/recharge changes are expected to occur gradually or randomly rather than through the step change assumed in this analysis. However, such simple representations would facilitate our fundamental understanding of various complex impacts of climatic changes on contaminant concentrations and exports.

For the conditions explored in this study (Fig. 3) we expect that the changes in the recharge rates (as described in the scenarios above) will impact the concentration breakthrough curves (BTCs) by local dilution

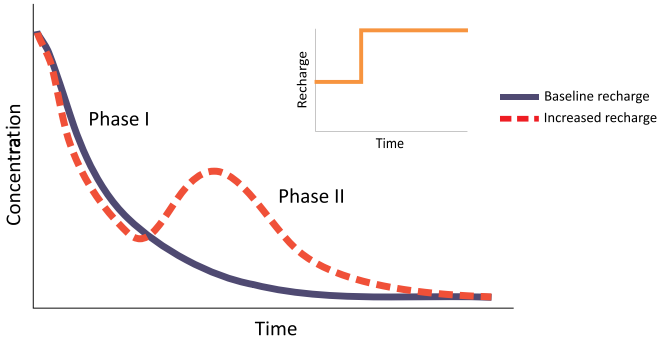

Fig. 4. Schematic illustration of the impact of increased recharge on the concentration breakthrough curve (BTC) at an observation well located downgradient from the source zone. The recharge rate increase causes a slight dilution (Phase I), followed by a "rebound" effect in the BTC (Phase II) due to contaminants' mobilization. The continuous blue curve indicates the BTC under baseline recharge whereas the dashed red curve corresponds to the concentration BTC under a change in the recharge conditions (see inset figure). (For interpretation of the references to colour in this figure legend, the reader is referred to the web version of this article.)

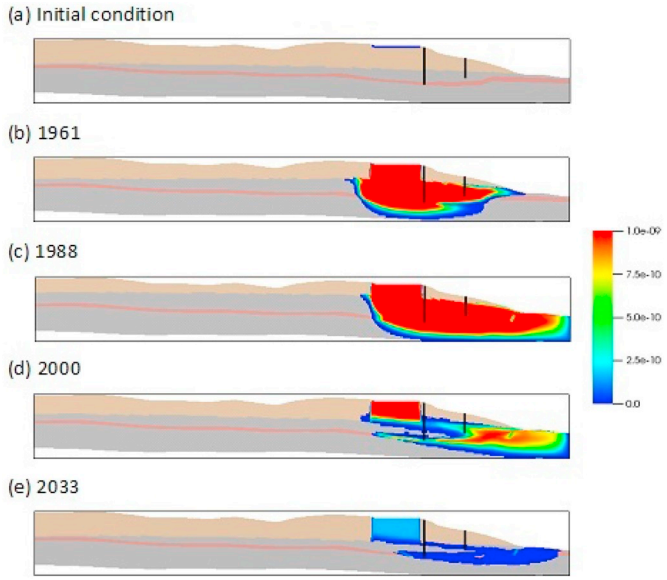

Fig. 5. Illustration of the simulated tritium plume in the SRS. The initial condition is displayed in panel (a). The plume snapshots are shown for years (b) 1961, (b) 1988, (c) 2000 and (d) 2033.

as well as by affecting the rate at which the contaminant mass is released from the vadose zone to the groundwater system. Fig. 4 schematically pictures the contaminant BTC under baseline conditions and perturbed recharge conditions. We expect that, increased recharge (relative to the baseline values) causes a slight dilution (Phase I in Fig. 4) followed by a "rebound" effect in the concentration BTC (Phase II in Fig. 4) due to the mobilization of the solute mass located in proximity of the source (Fig. 4).

4. Results and discussion

4.1. Spatiotemporal dynamics of the contaminant plume

Prior to investigating the effects of recharge on transport observables at specific wells and at the CP, we provide snapshots of the simulated contaminant plume in the coupled vadose zone-groundwater system (Fig. 5) for the baseline case. Fig. 5 shows the plume migration at different years, namely 1961 (Fig. 5b), 1988 (Fig. 5c), 2000 (Fig. 5d) and 2033 (Fig. 5e).

As observed in Bea et al. (2013), the contaminant plume first moves downward in the vadose zone, and then spreads laterally below the groundwater table (Fig. 5b). During the operation, most of the plume migrates within the upper aquifer, although a part of the plume penetrates the TCCZ and reaches the lower aquifer (Fig. 5c). After the operation ends, the clean water front arrives from upstream and pushes the plume downgradient (Fig. 5d). The contaminant plume displays a stratified distribution since the residual contaminants in the vadose zone constitute a persistent contamination source and the low-permeability TCCZ becomes a secondary source. As displayed in Fig. 5e, in year 2033 the vadose zone and TCCZ continue to be the residual contaminant sources.

4.2. Contaminant concentration and export BTCs

We first compare the temporal evolution of the ^{3}H concentrations [mol kgw^{-1}] at the observation wells and of the ^{3}H export [mol y^{-1}] at the CP among different recharge scenarios (Figs. 6–9) for 0–100 years forward from the assumed recharge perturbations and cap failure (i.e., within the timeframe 2020–2100). Under baseline recharge conditions (indiated by $\epsilon = 0$ in Figs. 6–9), ^{3}H concentrations and export generally

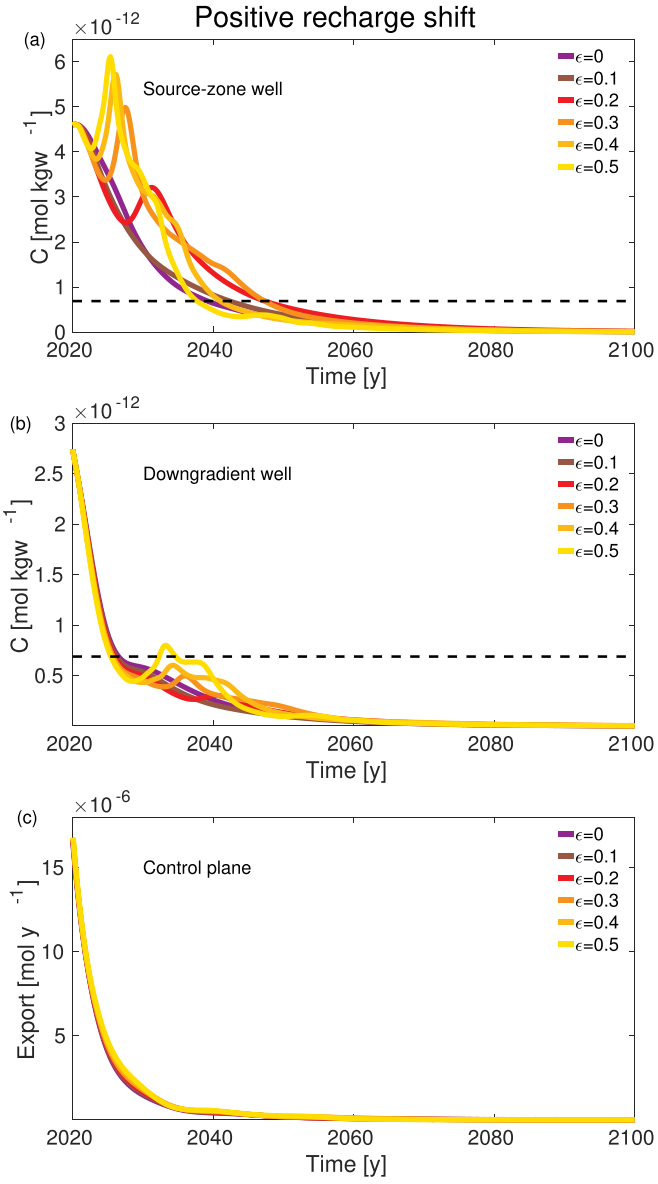

Fig. 6. Temporal evolution of ^{3}H concentration at the: (a) source-zone well, (b) downgradient well and (c) ^{3}H export at the CP for the baseline scenario, indicated by $\epsilon = 0$, and the constant positive recharge shift scenario, characterized by $\epsilon = 0.1,0.2,0.3,0.4,0.5$. The results of different recharge perturbations are portrayed in different colors. The thin horizontal dashed black line represents the MCL for ^{3}H.

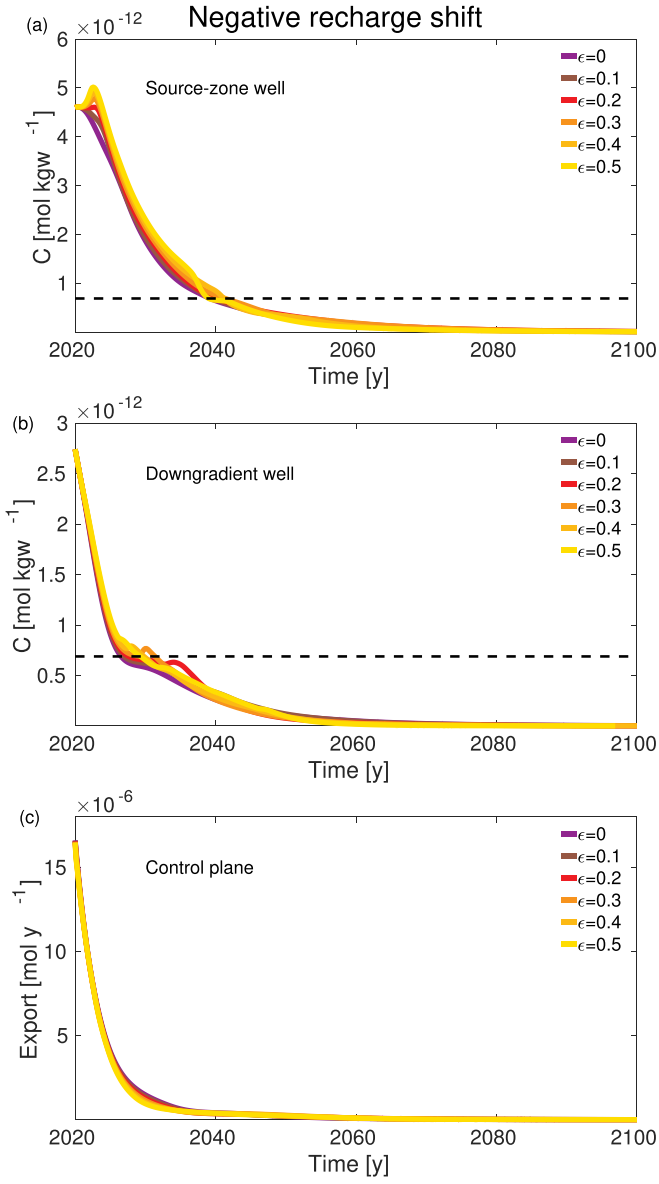

Fig. 7. Temporal evolution of ^{3}H concentration at the: (a) source-zone well, (b) downgradient well and (c) ^{3}H export at the CP for the baseline scenario, indicated by $\epsilon = 0$, and the constant negative recharge shift scenario, characterized by $\epsilon = 0.1,0.2,0.3,0.4,0.5$. The results of different recharge perturbations are portrayed in different colors. The thin horizontal dashed black line represents the MCL for ^{3}H.

decrease within the timeframe 2020–2100, given that the peak concentration and export occur closer to the contaminant discharge operation timeframe (1955–1988), i.e., before year 2020.

When the positive constant shift of recharge occurs (Fig. 6), the concentration initially decreases for approximately 2–10 years at the source-zone well (Fig. 6a) and for around 5–20 years at the downgradient well (Fig. 6b). This slight decrease of concentration is an outcome of dilution, attributed to the presence of more water in the system which enhances the mixing of the plume with clean water. We then observe a "rebound" in the concentrations due to the additional recharge, during which the concentration increases with respect to the concentration BTC obtained for the baseline case ($\epsilon = 0$). This is attributed to the fact that the residual contaminants in the vadose zone are mobilized under higher recharge. As a consequence, more solute mass reaches the wells and the CP. The concentration increase during the "rebound" phase is more pronounced at the source-zone well (Fig. 6a) than at the downgradient well (Fig. 6b) given that the latter is located further away from the source zone and consequently less influenced by the mobilization of residual ^{3}H. These results are in agreement with previous theoretical analysis which showed that near-source locations are more sensitive to changes in the solute mass release at the source zone (de Barros, 2018). By comparing the effects of different magnitudes of recharge shifts on well concentrations, we notice that a recharge increase characterized by $\epsilon = 0.1$ does not influence the concentration BTC significantly. On the other hand, Fig. 6a and b show that, for larger recharge, the timing of the "rebound" effect happens before and the corresponding peak concentration is higher (i.e., see concentration BTCs within the range $\epsilon = 0.2 - 0.5$). We also point out that the concentration decrease after the peak is generally more rapid as ϵ increases (see BTCs produced by $\epsilon = 0.4 - 0.5$ in Fig. 6a–b). Indeed, under higher recharge, a bigger part of the residual ^{3}H is mobilized and flushed out of the aquifer system earlier in time. The export, on the

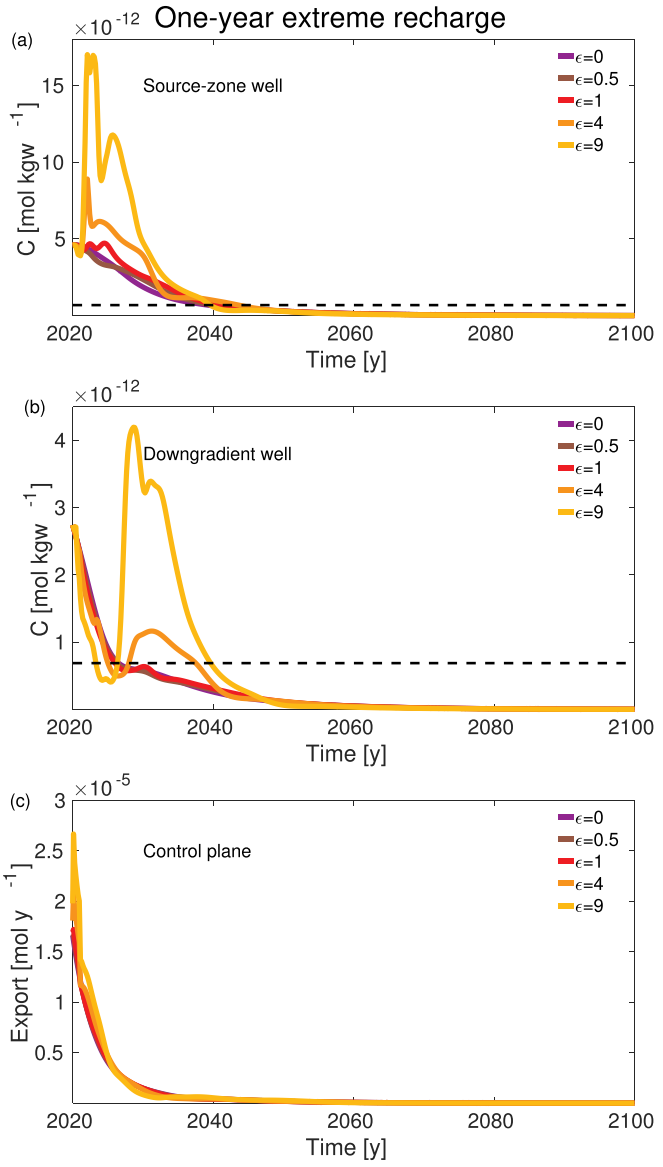

Fig. 8. Temporal evolution of ^{3}H concentration at the: (a) source-zone well, (b) downgradient well and (c) ^{3}H export at the CP for the baseline scenario, indicated by $\epsilon = 0$, and the one-year extreme recharge scenario, characterized by $\epsilon = 0.5,1,4,9$. The results of different recharge perturbations are portrayed in different colors. The thin horizontal dashed black line represents the MCL for ^{3}H.

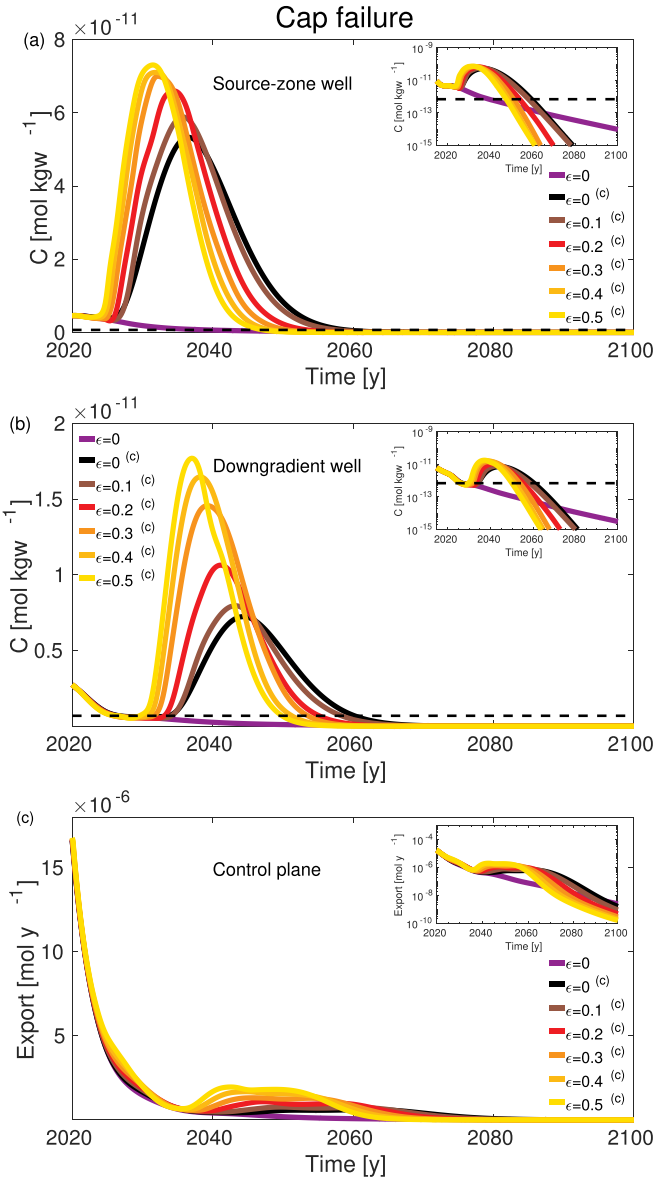

Fig. 9. Temporal evolution of ^{3}H concentration at the: (a) source-zone well, (b) downgradient well and (c) ^{3}H export at the CP for the baseline scenario, indicated by $\epsilon = 0$, the cap failure under the baseline scenario, indicated by $\epsilon = 0^{(c)}$, and the cap failure under the constant positive recharge shift scenario, indicated by $\epsilon = 0.1^{(c)},0.2^{(c)},0.3^{(c)},0.4^{(c)},0.5^{(c)}$, with $^{(c)}$ indicating the capping failure. The results of different recharge perturbations are portrayed in different colors. The thin horizontal dashed black line represents the MCL for ^3H. The inset shows the log-scale plot.

other hand, slightly tends to increase but does not change significantly even under the maximum increase of recharge, indicated by $\epsilon = 0.5$ (Fig. 6c). The minor effects on the export are attributed to the fact that the export is an integrated measure that incorporates the upwelling groundwater from the lower aquifer which is less affected by the recharge changes.

Decreased recharge (Fig. 7) produces minor effects on well concentrations compared to increased recharge (compare Fig. 6a–b to Fig. 7a–b). Lower recharge causes a small increase in the concentration for around 5–20 years at the source-zone well (Fig. 7a) and for approximately 10–20 years at the downgradient well (Fig. 7b). Fig. 7a depicts a higher peak concentration as ϵ increases. This effect takes place because a lower amount of water in the system decreases the dilution potential of the aquifer hence leading to an increase the concentration. The differences between the concentration BTCs obtained for different ϵ values at both observation wells in Fig. 7a–b are less visible than in Fig. 6a–b. We observe that increased recharge has a larger impact on the source-zone well (Fig. 7a) than on the downgradient well (Fig. 7b), whereas decreased recharge causes more uniform effects between the two observation wells. This is because the mobilization of ^{3}H caused by increased recharge has more impact closer to the source (Fig. 7a), whereas the decrease of dilution, emerging from decreased recharge and resulting in higher concentration (Fig. 7a–b) has a more uniform effect on the aquifer system. Finally, minor effects are displayed on the export (Fig. 7c), as noted also for increased recharge conditions (see Fig. 6c). However we notice that the ^{3}H export tends to slightly decrease under negative recharge shifts given that less residual ^{3}H is mobilized from the vadose zone.

We next observe the outcomes of the third scenario (i.e., the one-year extreme recharge event) in Fig. 8. One-year of extreme recharge

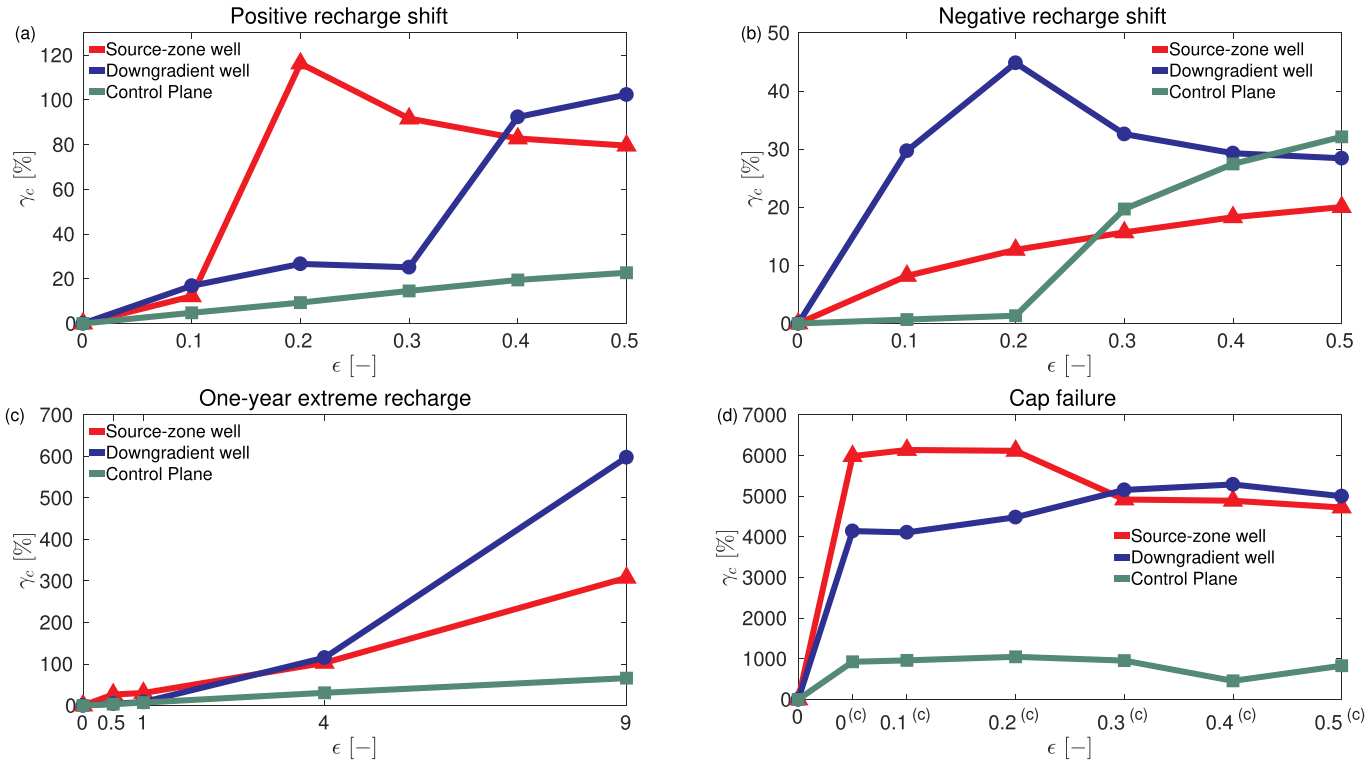

Fig. 10. Maximum difference between contaminant concentrations and export BTCs of the baseline scenario and the perturbed recharge scenarios (γ_c) versus perturbation (ϵ) for the constant positive recharge shift scenario (a), the constant negative recharge shift scenario (b), the one-year extreme recharge scenario (c), the cap failure and constant positive recharge shift scenario (d), where the superscript $^{(c)}$ indicates the capping failure. Results at the source-zone well are illustrated in red, at the downgradient well are pictured in blue and at the CP are indicated in green. (For interpretation of the references to colour in this figure legend, the reader is referred to the web version of this article.)

significantly increases the well concentrations during the "rebound" phase over an extended period of time, i.e., for around 10–20 years (Fig. 8a–b). We then observe that a short extreme event could affect the well concentrations for several decades. At the source-zone well (Fig. 8a), prior to the "rebound" phase, the concentration decreases slightly after the perturbation event (in 2020) due to dilution, particularly under the most extreme scenario, indicated by $\epsilon = 9$. On the other hand, at the downgradient well (Fig. 8b), the concentration decrease due to dilution is more pronounced given that the plume has traveled a longer distance. Five-to-ten years after the initial dilution, the concentration increases, during the "rebound" phase. The extreme one-year precipitation indicated by $\epsilon = 0.5$ does not significantly affect the concentrations, especially at the downgradient well, where even the recharge scenario characterized by $\epsilon = 1$ does not produce significant changes when compared to baseline conditions ($\epsilon = 0$). We also observe that higher recharge shifts produce higher peak concentrations in the "rebound" phase due to the mobilization of the solute mass at the source zone (Fig. 8a–b) as well as higher initial dilution. The effect of recharge changes on the export (Fig. 7c) is minor compared to the influence on the concentrations in the wells (Fig. 8a–b), although we observe a peak of the export around 2020 when $\epsilon = 9$.

Fig. 9 reports the results obtained for the scenario characterized by the failure of the capping structure under baseline conditions and constant positive recharge shifts starting in 2020. Fig. 9 shows that the concentration increase at the wells is significantly larger than the increase observed for undamaged source-zone capping conditions. The concentration "rebound" happens after 5–8 years at the source-zone well (Fig. 9a) and after 10–15 years at the downgradient wells (Fig. 9b). The export at the CP also shows a visible increase after around 2035 (Fig. 9c). This is due to the fact that, under higher recharge and no capping structure, the bulk of residual contaminants in the vadose zone migrate to the groundwater system. We notice that the increase of concentration/export happens earlier in time at the well closer to the contaminant source zone, later at the downgradient well and even further when considering the export at the CP, located at the right boundary of the domain. Moreover, as the recharge value increases, from $\epsilon = 0.1$ to $\epsilon = 0.5$, the peak concentration/export, caused by the additional recharge, becomes higher and occurs earlier in time (see Fig. 9). The inset log-scale plot of Fig. 9a shows that the extreme concentration increase resulting from the cap failure is followed by a rapid decrease of the concentration, as the ^{3}H plume is flushed out of the system earlier when the capping structure fails, moving the contamination problem downgradient. This effect is amplified as ϵ increases. The same observations apply to the downgradient well and to the export (see inset log-scale plot of Fig. 9b–c). We finally notice that the difference between the BTCs given by different ϵ values is more pronounced when we assume that the cap fails (Fig. 9).

The results of an additional recharge scenario, characterized by a range of positive recharge shifts within a timeframe shorter than a year, is presented in the Supplementary Material. These outcomes confirm that our findings also apply to a smaller time scale of hydrological shift.

4.3. Impact of recharge perturbations on key environmental performance metrics

We quantify the impact of climate change-driven recharge shifts on key EPMs (e.g, peak contaminant concentration, early and late arrival times, time of exceedance of MCL). Given that the recharge shifts considered in our study start from year 2020 (after the discharge operation at the SRS F-Area terminated, i.e. during a contaminant concentration/export descending/tailing phase), we do not consider the peak concentration but we analyze the maximum change on the concentration and export BTCs induced by the recharge perturbations. Moreover we investigate the effect of recharge shifts on the time of

exceedance of the MCL for ^{3}H.

4.3.1. Maximum difference between baseline and perturbed BTCs

We identify the maximum normalized difference between the contaminant concentration or export BTC obtained under baseline and perturbed recharge conditions as:

$$\gamma_c = \frac{1}{C_b(t_{d_{max}})} \max_t |C_b(t) - C_p(t)| \times 100, \quad (5)$$

where $C_b(t)$ and $C_p(t)$ in (5) are the contaminant concentration [mol kgw^{-1}] or contaminant export [mol y^{-1}] of the baseline (subscript "b") and the perturbed (subscript "p") recharge scenarios respectively, whereas $C_b(t_{d_{max}})$ is the baseline concentration or export taken at the time where the difference between baseline and perturbed BTCs is maximum. The metric γ_c (5) is plotted in Fig. 10 as a function of the recharge perturbation ϵ, whose values are described in Section 3.2. Note that, from (5), $\gamma_c = 0$ for the baseline scenario, indicated by $\epsilon = 0$. We recall that only a limited range of recharge perturbations were simulated in our analysis, therefore the comments below are based on a linear interpolation between γ_c and the analyzed ϵ values.

When the recharge is positively shifted by a constant value (Fig. 10a), the relative change in the well concentrations, quantified by γ_c (5), exhibit a non-linear or step-function response to the perturbation ϵ. As shown in Fig. 10a, γ_c at the source-zone well drastically increases (from around 10% to almost 120%) when the recharge perturbation ϵ changes from 0.1 to 0.2, while γ_c at the downgradient well is highly impacted (it changes from approximately 20% to 100%) when ϵ goes from 0.3 to 0.4. The changes are smaller during the other recharge shifts' intervals. Our results suggest the presence of a threshold, or trigger level of recharge, above which the well concentrations are significantly affected. This trigger level is lower at the source-zone well than at the downgradient well; a recharge corresponding to $\epsilon = 0.1$ could represent this threshold at wells closer to the source-zone, while a higher trigger level of recharge, approximately identified by $\epsilon = 0.3$, is identified downgradient. The export, on the other hand, increases in a quasi-linear manner with the recharge perturbation (Fig. 10a). As shown in the concentration time series (see Fig. 6c), the effect of recharge shifts on the export is significantly smaller compared to that on the well concentrations. Indeed a recharge shift corresponding to $\epsilon = 0.5$ results in a value of γ_c of approximately 20% when observing the CP export, while a recharge shift given by $\epsilon = 0.5$ produces values of γ_c of approximately 80%–100% at the observation wells.

Fig. 10b shows the $\gamma_c - \epsilon$ relationship for the negative recharge shift scenario. Decreasing the recharge rate generally has a smaller impact on γ_c with respect to increased recharge conditions (compare the values of γ_c in Fig. 10a and b), according to the results in Fig. 7. We identify non-linear responses and trigger levels of recharge perturbation at the downgradient well and at the CP. The trigger levels are very small at the downgradient well (e.g., less than $\epsilon = 0.1$) and higher for the export (i.e., $\epsilon = 0.2$). The maximum difference between the baseline case and the perturbed BTC (computed via Eq. (5)) is larger at the downgradient well than at the source-zone well (see Fig. 10b). This is different than what was observed from the results of the positive shift scenario. When comparing Fig. 10a and b we observe that, under positive shifts of recharge (Fig. 10a), γ_c evaluated at the source-zone is more sensitive to smaller ϵ values. In other terms, we could say that the source-zone well responds first to the perturbation ϵ. This is because the source-zone well is more impacted by the mobilization of ^3H given its proximity to the source. However, when the recharge decreases (Fig. 10b), changes in γ_c are more prominent at the downgradient well for smaller perturbations ϵ, i.e., the downgradient well responds first than the source-zone well. Indeed, the changes in the concentration are more uniform between the source-zone well and the downgradient well (compare Fig. 7a and b) under lower recharge because they happen due to the concentration (or less dilution) as opposed to the mobilization of contaminants. Moreover, these changes take place at a later time downgradient, when the baseline concentration is smaller, resulting in higher γ_c downgradient.

Under the extreme one-year recharge scenario (Fig. 10c), the trigger-level is larger (around $\epsilon = 1$) when compared to the results obtained for the constant positive recharge shift scenario at both observation wells (compare Fig. 10a and c). We observe that the γ_c-ϵ relationship is quite similar for the two observation wells until $\epsilon = 4$. However, when $\epsilon = 9$, the recharge increase impact at the downgradient well becomes quite significant. In quantitative terms, this impact is approximately two times that at the source zone well (compare red and blue lines in Fig. 10c). Finally, the impact of the extreme event on the contaminant export is quite limited and increases linearly with the perturbation ϵ (Fig. 10c). However, a significant increase of the export is detected for the most extreme one-year precipitation event investigated in this study (i.e., when $\epsilon = 9$, γ_c equals 65%).

The cap failure scenario (Fig. 10d) also shows a non-linear response when evaluating the sensitivities of the wells' concentrations and the export to the perturbation ϵ. We observe an extreme increase of γ_c caused by the signification mobilization of the residual contaminants entrapped in the vadose zone when the capping structure fails, confirming the importance of the latter containment system. Successive increases of recharge do not significantly affect the value of γ_c, i.e., γ_c reaches a plateau under capping failure conditions. The almost constant value of γ_c is generally higher at the source-zone well than at the donwgradient well and at the CP. Our analysis then suggests that the failure of the capping can be identified as a trigger situation after which major changes in both well concentrations and on the export are expected.

4.3.2. Difference of time above MCL between baseline and perturbed BTCs

In this Section, we identify the metric γ_t as the normalized difference of the time of exceedance of the MCL for ^3H between the baseline recharge scenario and the perturbed recharge scenarios as:

$$\gamma_t = \frac{1}{t(C_b(t) > MCL)} |t(C_b(t) > MCL) - t(C_p(t) > MCL)| \times 100, \quad (6)$$

with $t(C_b(t) > MCL)$ and $t(C_p(t) > MCL)$ respectively being the time [d] during which the contaminant concentration exceeds the EPA's MCL for ^3H for the baseline (subscript "b") and the perturbed (subscript "p") recharge scenarios. As before, the metric γ_t (6), expressed in percentage, is plotted as a function of ϵ for each recharge scenario in Fig. 11 and, from (6), $\gamma_t = 0$ for the baseline scenario (i.e., when $\epsilon = 0$). Similarly to before, our observations are based on a linear interpolation between γ_t and the range of ϵ values considered.

Under the positive shift of recharge scenario (Fig. 11a), γ_t shows a non-linear response to the recharge perturbation ϵ at the source-zone well (in red). In this case, γ_t increases until its maximum value under a perturbation $\epsilon = 0.2$ and $\epsilon = 0.3$ but decreases afterwards. We then notice that the intermediate values of ϵ produce the highest influence on the timeframe of MCL exceedance, as compared to the highest values of ϵ. Indeed, positive recharge shifts initially dilute the plume in the tailing phase, and increase the ^{3}H mobilization, leading to an increase of the concentration during the "rebound" phase, but afterwards flush the plume out of the system, i.e., at a later stage the ^{3}H concentration values reach the ^{3}H MCL faster (see BTCs characterized by $\epsilon = 0.4 - 0.5$ in Fig. 6a). The higher the recharge, the higher is the concentration "rebound" peak and the faster the plume is flushed out of the aquifer, therefore the maximum increase of the time above MCL is produced by intermediate value of recharge (for example given by $\epsilon = 0.2, 0.3$). On the other hand, γ_t (6) increases almost linearly with the permanent positive recharge perturbation at the downgradient well (in blue) but the maximum change of γ_t (6) with respect to the baseline recharge scenario is only around 15%.

Decreased recharge (Fig. 11b) also results in a non-linear response of γ_t to ϵ. Compared to the positive recharge shift scenario in which the source-zone well responds first (Fig. 11a), when the recharge is negatively shifted (Fig. 11b), the downgradient well responds first. A

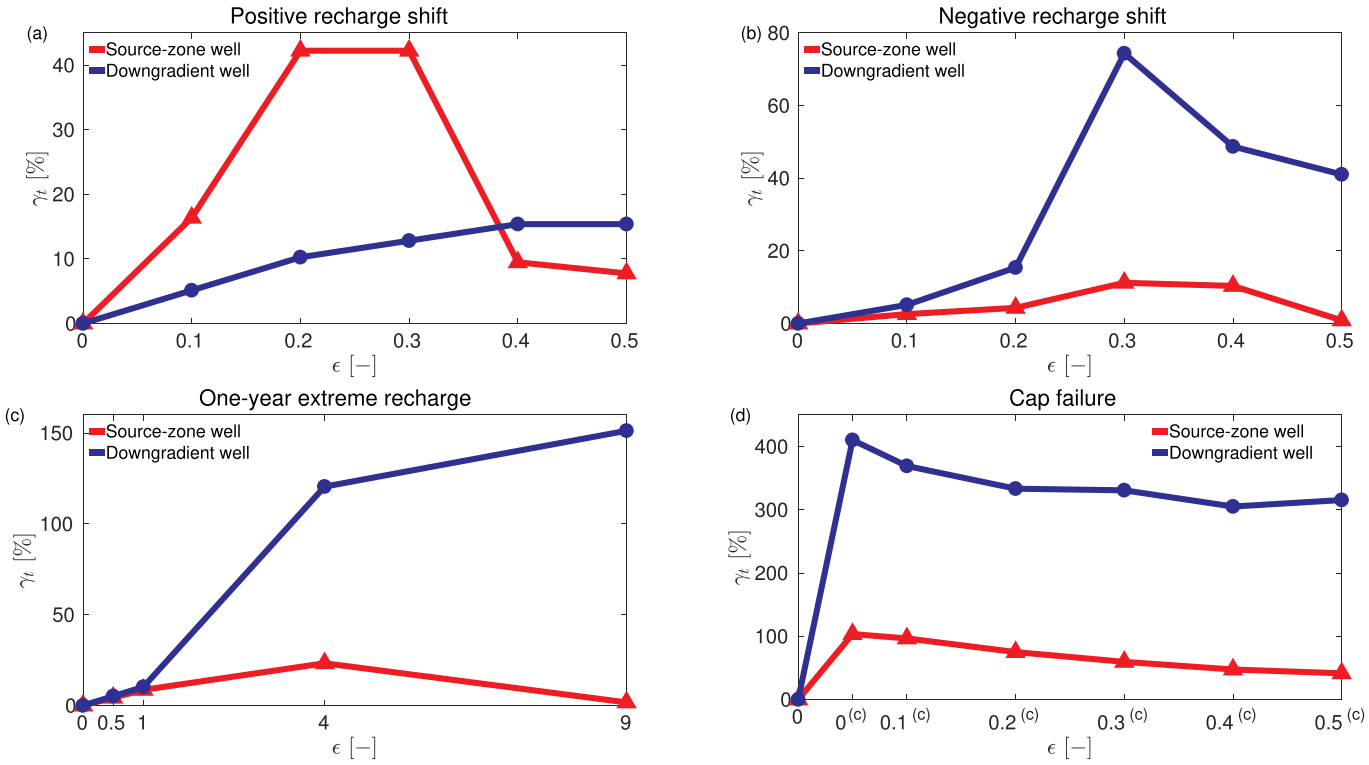

Fig. 11. Difference of time of exceedance of the MCL for ^3H between the baseline scenario and the perturbed recharge scenarios (γ_t) versus perturbation (ϵ) for the constant positive recharge shift scenario (a), the constant negative recharge shift scenario (b), the one-year extreme recharge scenario (c), the cap failure and constant positive recharge shift scenario (d), where the superscript $^{(c)}$ indicates the capping failure. Results at the source-zone well are illustrated in red and results at the downgradient well are pictured in blue. (For interpretation of the references to colour in this figure legend, the reader is referred to the web version of this article.)

decrease of the natural recharge does not significantly influence the time when the ^{3}H concentration exceeds MCL at the source-zone well (in red) given that the minor concentration increase takes place when the baseline concentration exceeds the MCL. However we identify the value of $\epsilon = 0.2$ as the trigger level of recharge decrease after which the time above MCL is significantly affected at the downgradient well (in blue). The remaining recharge steps produce less significant changes at the downgradient well.

One-year of extreme recharge produces relatively smaller changes in the time above MCL as compared to the effect of permanent shifts of recharge when $\epsilon < 1$ (compare Fig. 11c with Fig. 11a). This scenario does not influence much the time of MCL exceedance at the source-zone well (in red), where a maximum γ_t around 20% is identified when $\epsilon = 4$. Nevertheless, the response at the downgradient well, also non-linear, shows a trigger level represented by $\epsilon = 1$ above which the time of exceedance of MCL is highly impacted. This significant impact takes place because the increase of concentration downgradient, which results in values above the ^{3}H MCL, happens later in time, compared to the upgradient well, when the baseline concentration is already below the MCL.

When the capping structure fails (Fig. 11d), we notice that γ_t reaches the maximum value at both wells, similarly to what observed when looking at the $\gamma_c - \epsilon$ results. The value of γ_t then decreases at both wells when the recharge increases in the presence of no cap. This decrease is almost linear at the source-zone well. In the overall, we observe that the capping failure is identified as a trigger condition which causes an important increase of both EPMs (as quantified by γ_c and γ_t), therefore a substantial risk increase.

When comparing the results in Figs. 10 and 11 we understand that different recharge's thresholds/trigger levels are identified depending on the metric of interest for environmental remediation (for instance the maximum concentration/export BTC's change or the time of exceedance of MCL's change caused by the recharge perturbations), the location of the observation location and the measured variable (e.g., contaminant concentration or contaminant export).

5. Summary and conclusions

In this paper we investigate the impact of climate change-driven aquifer's recharge shifts on residual contaminants in soil and groundwater subject to sustainable remediation. For the sake of simplicity we assume that the changes in precipitation and temperature can be translated into changes of the natural aquifer's recharge. We establish the evaluation methodology, including the development of potential future scenarios on the basis of national climate assessments, site-specific model developments, and evaluation criteria. We illustrate four scenarios characterized by a range of variable recharge values: (1) constant positive recharge shift after a certain year (2) constant negative recharge shift after a certain year, (3) one-year of extreme recharge, (4) cap failure and constant positive recharge shift. Our methodology is demonstrated by simulating the ^{3}H plume migration within the US DOE's nuclear reservation Savannah River Site F-Area. We employ the unsaturated-saturated flow model Amanzi, calibrated and verified using site data.

In summary, our results generally show that changes of the recharge regime (even small) can significantly affect contaminant concentrations. The most noticeable outcome is the concentration “rebound” effect taking place, after an initial slight dilution, under higher recharge and/or capping failure conditions, which is given by the mobilization of the contaminant mass from the source zone and its transfer to the aquifer system. The concentration “rebound” effect is more pronounced and happens earlier as the recharge perturbation increases. Decreased recharge conditions could also cause a small concentration increase attributed to a decrease in the dilution potential of the aquifer. On the other hand, the ^{3}H export at the CP is only minimally influenced by recharge shifts, except for some extreme recharge scenarios. Trigger

levels of recharge which highly impact the concentration BTC at the wells are identified. These threshold/trigger levels depend on the observation location and on the EPM under investigation, quantified through γ_c and γ_t. The latter display a non-linear response to the perturbation ϵ. For example, it is interesting to observe that the most significant influence on the time of exceedance of MCL under positive recharge shifts (i.e., first scenario) is identified under recharge values in the middle of the range considered given that higher ϵ values cause a steeper decrease of the concentration after the "rebound" phase, i.e., the concentration reaches the MCL faster.

Our results suggest that close monitoring of wells concentrations should be adopted during precipitation (connected to higher aquifers' recharge) and drought (connected to lower aquifers' recharge) periods, however the actual risk of the downgradient population, as quantified through the export, could be under control even when the well concentrations are remarkably impacted. Our findings constitute then immediate contribution to guide groundwater monitoring in the presence of increased climatic variabilities, particularly in explaining concentration anomalies. For example, without a proper understanding, the concentration increase, due to higher or lower recharge, could be mistaken, for instance attributed to additional leaks or contaminant sources. In addition, our analysis indicates that source-zone wells are critical to early detect mobilized residual contaminants under increased recharge or cap failure conditions. It would be advantageous to have more frequent sampling or in situ monitoring in the proximity of the contaminant source zones as an early warning system (Schmidt et al., 2018). Aside from monitoring the contaminant concentration, characterizing the hydraulic fluxes in the vicinity of the source zone can also aid in understanding the macro-dispersive behavior of the plume and corresponding risks to the environment and public health (de Barros and Nowak, 2010; Henri et al., 2016). Our work also emphasizes the importance of properly maintaining the capping structure not only to sequester residual contaminants but also to reduce the uncertainty associated with climate variability, in fact the difference among recharge scenarios is smaller when the cap is undamaged.

We finally highlight that currently, simplified models adopting conservative assumptions are often used for performance and risk assessments at contaminated sites. Conservative approaches usually assume the worst case scenario, associated with higher recharge rates or higher permeability values to increase the plume mobility. The modeling scenarios investigated in this work, however, call into question the appropriateness of such conservative approaches, in fact the non-trivial trade-offs arising from the interplay between dilution and contaminants' mobilization require the use of more realistic and accurate flow and transport simulations, achieved through proper calibration processes, as well as probabilistic risk assessments (Maxwell et al., 2008; de Barros and Rubin, 2008; Siirila and Maxwell, 2012; Atchley et al., 2013; Libera et al., 2017). Overall, the trade-offs identified in our work must be evaluated with respect to the specific time, location and performance metric under investigation. Understanding these trade-offs would enable better allocation of available resources towards reducing uncertainty in decision making (de Barros et al., 2009, 2012).

Our work could be expanded by considering a more complex geochemistry setting, as well as surface water processes (e.g., evapotranspiration), and land model components (e.g., vegetation) of the SRS F-Area. Additionally, this study would benefit from an inclusion of different conceptualization of the aquifer's heterogeneous properties together with remediation strategies located at the site (e.g., pump and treat, funnel and gate systems). In particular, the effect of geological heterogeneity should be explored in more detail given that it can significantly augment contaminant plume mixing rates (de Barros et al., 2015).

Acknowledgements

This material is based upon work supported as part of the ASCEM project, which is funded by the U.S. Department of Energy, Office of Environmental Management, and as part of the Lawrence Berkeley National Laboratory Science Focus Area, which is funded by the U.S. Department of Energy, Office of Science, Office of Biological and Environmental Research, both under Award Number DE-AC02-05CH11231 to Lawrence Berkeley National Laboratory. This research used resources of the National Energy Research Scientific Computing Center, a DOE Office of Science User Facility supported by the Office of Science of the U.S. Department of Energy under Contract No. DE-AC02-05CH11231. We thank Christiana Patricola for her valuable advice on climate data and assumptions. The first and second authors acknowledge the support by the National Science Foundation under Grant No. 1654009. Finally, we thank two anonymous reviewers for the constructive comments.

Appendix A. Supplementary data

Supplementary data to this article can be found online at https://doi.org/10.1016/j.jconhyd.2019.103518.

References

Atchley, A.L., Maxwell, R.M., Navarre-Sitchler, A.K., 2013. Human health risk assessment of CO2 leakage into overlying aquifers using a stochastic, geochemical reactive transport approach. Environ. Sci. Technol. 47 (11), 5954–5962.
Bea, S.A., Wainwright, H., Spycher, N., Faybishenko, B., Hubbard, S.S., Denham, M.E., 2013. Identifying key controls on the behavior of an acidic-U (VI) plume in the Savannah River site using reactive transport modeling. J. Contam. Hydrol. 151, 34–54.
Bloomfield, J.P., Williams, R.J., Gooddy, D.C., Cape, J.N., Guha, P., 2006. Impacts of climate change on the fate and behaviour of pesticides in surface and groundwater-a UK perspective. Sci. Total Environ. 369 (1–3), 163–177.
da Veiga, L.B., Lipnikov, K., Manzini, G., 2014. The Mimetic Finite Difference Method for Elliptic Problems. vol. 11 Springer.
Dai, M., Kelley, J.M., Buesseler, K.O., 2002. Sources and migration of plutonium in groundwater at the Savannah River site. Environ. Sci. Technol. 36 (17), 3690–3699.
Darracq, A., Greffe, F., Hannerz, F., Destouni, G., Cvetkovic, V., 2005. Nutrient transport scenarios in a changing Stockholm and Malaren valley region, Sweden. Water Sci. Technol. 51 (3–4), 31–38.
de Barros, F.P.J., 2018. Evaluating the combined effects of source zone mass release rates and aquifer heterogeneity on solute discharge uncertainty. Adv. Water Resour. 117, 140–150.
de Barros, F.P.J., Nowak, W., 2010. On the link between contaminant source release conditions and plume prediction uncertainty. J. Contam. Hydrol. 116 (1–4), 24–34.
de Barros, F.P.J., Rubin, Y., 2008. A risk-driven approach for subsurface site characterization. Water Resour. Res. 44 (1), 1–14.
de Barros, F.P.J., Rubin, Y., Maxwell, R.M., 2009. The concept of comparative information yield curves and its application to risk-based site characterization. Water Resour. Res. 45 (6), 1–16.
de Barros, F.P.J., Ezzedine, S., Rubin, Y., 2012. Impact of hydrogeological data on measures of uncertainty, site characterization and environmental performance metrics. Adv. Water Resour. 36, 51–63.
de Barros, F.P.J., Fiori, A., Boso, F., Bellin, A., 2015. A theoretical framework for modeling dilution enhancement of non-reactive solutes in heterogeneous porous media. J. Contam. Hydrol. 175-176, 72–83.
Denham, M., Eddy-Dilek, C., 2017. Influences on effective decay rates of radionuclides in groundwater: F-Area Seepage Basins, Savannah River site. In: WM2017 Conf. Phoenix, Arizona, USA.
Destouni, G., Darracq, A., 2009. Nutrient cycling and N2O emissions in a changing climate: the subsurface water system role. Environ. Res. Lett. 4 (035008), 1–7.
Easterling, D.R., Kunkel, K., Arnold, J., Knutson, T., LeGrande, A., Leung, L.R., Vose, R., Waliser, D., Wehner, M., 2017. Precipitation Change in the United States. https://science2017.globalchange.gov/chapter/front-matter-about/.
Ellis, D.E., Hadley, P.W., 2009. Sustainable remediation white paper-integrating sustainable principles, practices, and metrics into remediation projects. Remediat. J. 19 (3), 5–114.
Famiglietti, J.S., 2014. The global groundwater crisis. Nat. Clim. Chang. 4 (11), 945–948.
Faybishenko, B., Wainwright, H., Denham, M., Amidon, M., Millings, M., Flach, G., Eddy-Dilek, C., 2018. Basic climatic and hydrological data mining and analytics of the Savannah River site F-area. In: Report LBNL-2001173, Lawrence Berkeley National Laboratory, Berkeley, Calif., July 2018.
Flach, G., 2004. Groundwater Flow Model of the General Separations Area Using Porflow (U). WSRC-TR-2004-00106. Westinghouse Savannah River Company LLC, Savannah River Site, Aiken (SC 29808).
Flach, G.P., Crisman, S.a., Molz, F.J., 2004. Comparison of single-domain and dual-domain subsurface transport models. Ground Water 42 (6–7), 815–828.
Freshley, M., Hubbard, S.S., Flach, G., Freedman, V., Agarwal, D., Andre, B., Bott, Y., Chen, X., Davis, J., Faybishenko, B., Gorton, I., Murray, C., Moulton, D., Meyer, J., Rockhold, M., Shoshani, A., Steefel, C., Wainwright, H., Waichler, S., 2012. Phase II

Demonstration ASCEM United States Department of Energy.
Futter, M.N., Helliwell, R.C., Hutchins, M., Aherne, J., 2009. Modelling the effects of changing climate and nitrogen deposition on nitrate dynamics in a Scottish mountain catchment. Hydrol. Res. 40 (2–3), 153.
Gellens, D., Roulin, E., 1998. Streamflow response of Belgian catchments to IPCC climate change scenarios. J. Hydrol. 210 (1–4), 242–258.
Green, T.R., Taniguchi, M., Kooi, H., Gurdak, J.J., Allen, D.M., Hiscock, K.M., Treidel, H., Aureli, A., 2011. Beneath the surface of global change: impacts of climate change on groundwater. J. Hydrol. 405 (3–4), 532–560.
Henri, C.V., Fernàndez-Garcia, D., de Barros, F.P., 2016. Assessing the joint impact of DNAPL source-zone behavior and degradation products on the probabilistic characterization of human health risk. Adv. Water Resour. 88 (May), 124–138.
Killian, T.H., Kolb, N.L., Corbo, P., Marine, I.W., 1986. Environmental information document, F-area seepage basins. In: Report No. DPST 85–704.E.I. du Pont de Nemours & Co, Savannah River Laboratory, Aiken SC 29808.
Li, R., Merchant, J.W., 2013. Modeling vulnerability of groundwater to pollution under future scenarios of climate change and biofuels-related land use change: a case study in North Dakota, USA. Sci. Total Environ. 447, 32–45.
Libera, A., de Barros, F.P., Guadagnini, A., 2017. Influence of pumping operational schedule on solute concentrations at a well in randomly heterogeneous aquifers. J. Hydrol. 546, 490–502.
Lipnikov, K., Svyatskiy, D., Vassilevski, Y., 2010. A monotone finite volume method for advection-diffusion equations on unstructured polygonal meshes. J. Comput. Phys. 229 (11), 4017–4032.
Maxwell, R.M., Kastenberg, W.E., 1999. Stochastic environmental risk analysis: an integrated methodology for predicting cancer risk from contaminated groundwater. Stoch. Env. Res. Risk A. 13 (1–2), 27–47.
Maxwell, R.M., Carle, S.F., Tompson, A.F.B., 2008. Contamination, risk, and heterogeneity: on the effectiveness of aquifer remediation. Environ. Geol. 54 (8), 1771–1786.
Middelkoop, H., Daamen, K., Gellens, D., Grabs, W., Kwadijk, J.C.J., Lang, H., Parmet, B.W.A.H., Schadler, B., Schulla, J., Wilke, K., 2001. Impact of climate change on hydrological regimes and water resources management in the Rhine basin. Clim. Chang. 49 (1–2), 105–128.
Mualem, Y., 1976. A new model for predicting the hydraulic conductivity of unsaturated porous media. Water Resour. Res. 12 (3), 513–522.
O'Connell, S., Hou, D., 2015a. Resilience: a new consideration for environmental remediation in an era of climate change. Remediat. J. 26 (1), 57–67.
O'Connell, S., Hou, D., 2015b. Surfactant-oxidation co-application for soil and groundwater remediation. Remediat. J. 26 (1), 57–67.
Olesen, J.E., Carter, T.R., Díaz-Ambrona, C.H., Fronzek, S., Heidmann, T., Hickler, T., Holt, T., Minguez, M.I., Morales, P., Palutikof, J.P., Quemada, M., Ruiz-Ramos, M., Rubæk, G.H., Sau, F., Smith, B., Sykes, M.T., 2007. Uncertainties in projected impacts of climate change on European agriculture and terrestrial ecosystems based on scenarios from regional climate models. Clim. Chang. 81 (Suppl. 1), 123–143.
Park, M.J., Park, J.Y., Shin, H.J., Lee, M.S., Park, G.A., Jung, I.K., Kim, S.J., 2010. Projection of future climate change impacts on nonpoint source pollution loads for a forest dominant dam watershed by reflecting future vegetation canopy in a soil and water assessment tool model. Water Sci. Technol. 61 (8), 1975–1986.
Pfister, L., Kwadijk, J., Musy, A., Bronstert, A., Hoffmann, L., 2004. Climate change, land use change and runoff prediction in the Rhine–meuse basins. River Res. Appl. 20 (3), 229–241.
Phifer, M., Millings, M., Flach, G., 2006. Hydraulic property data package for the e-area and z-area soils. In: Cementitious Materials and Waste Zones, Washington Savannah River Company, Savannah River Site, Aiken, South Carolina.
Sassen, D.S., Hubbard, S.S., Bea, S.A., Chen, J., Spycher, N., Denham, M.E., 2012. Reactive facies: an approach for parameterizing field-scale reactive transport models using geophysical methods. Water Resour. Res. 48 (10), 1–20.
Schiedek, D., Sundelin, B., Readman, J.W., Macdonald, R.W., 2007. Interactions between climate change and contaminants. Mar. Pollut. Bull. 54 (12), 1845–1856.
Schmidt, F., Wainwright, H.M., Faybishenko, B., Denham, M., Eddy-Dilek, C., 2018. In situ monitoring of groundwater contamination using the kalman filter. Environ. Sci. Technol. 52 (13), 7418–7425.
Siirila, E.R., Maxwell, R.M., 2012. A new perspective on human health risk assessment: development of a time dependent methodology and the effect of varying exposure durations. Sci. Total Environ. 431, 221–232.
Sjoeng, A.M.S., Kaste, O., Wright, R.F., 2009. Modelling future NO3 leaching from an upland headwater catchment in SW Norway using the MAGIC model: II. Simulation of future nitrate leaching given scenarios of climate change and nitrogen deposition. Hydrol. Res. 40 (2–3), 217–233.
Tokunaga, T.K., Wan, J., Denham, M.E., 2012. Estimates of vadose zone drainage from a capped seepage basin, F-Area, Savannah River site. Vadose Zone J. 11 (3).
US Environmental Protection Agency https://www.epa.gov/brownfields.
US Environmental Protection Agency https://www.epa.gov/superfund.
Van Bokhoven, A., 2006. The impact of climate change on the water quality of the Rhine river. Kiwa Water Res. 56, 423–440 *(147 pp.)*.
Van Vliet, M., Zwolsman, J., 2008. Impact of summer droughts on the water quality of the meuse river. J. Hydrol. 353 (1–2), 1–17.
Visser, A., Kroes, J., Van Vliet, M.T.H., Blenkinsop, S., Fowler, H.J., Broers, H.P., 2012. Climate change impacts on the leaching of a heavy metal contamination in a small lowland catchment. J. Contam. Hydrol. 127 (1–4), 47–64.
Wainwright, H.M., Chen, J., Sassen, D.S., Hubbard, S.S., 2014. Bayesian hierarchical approach and geophysical data sets for estimation of reactive facies over plume scales. Water Resour. Res. 50 (6), 4564–4584.
Wainwright, H., Molins, S., Davis, J., Arora, B., Faybishenko, B., Krishnan, H., Hubbard, S., Flach, G., Denham, M., Eddy-Dilek, C., 2015. Using ASCEM modeling and visualization to inform stakeholders of contaminant plume evolution and remediation efficacy at F-Basin Savannah River. In: SC. *WM2015 Conf*, pp. 1–14.
Wainwright, H., Faybishenko, B., Molins, S., Davis, J., Arora, B., Pau, G., Johnson, J., Flach, G., Denham, M., Eddy-dilek, C., Moulton, D., Lipnikov, K., Gable, C., Miller, T., Freshley, M., 2016. Effective long-term monitoring strategies by integrating reactive transport models with in situ geochemical measurements 16212. In: WM2016 Conf, pp. 1–15.
Whitehead, P., Wilby, R., Battarbee, R., Kernan, M., Wade, A.J., 2009. A review of the potential impacts of climate change on surface water quality. Hydrol. Sci. J. 54 (1), 101–123.
Wilby, R.L., Whitehead, P.G., Wade, A.J., Butterfield, D., Davis, R.J., Watts, G., 2006. Integrated modelling of climate change impacts on water resources and quality in a lowland catchment: river Kennet, UK. J. Hydrol. 330 (1–2), 204–220.
Worthy, W., Clarke, J.H., Abkowitz, M.D., 2013a. Near-surface disposal performance assessment: modeling monthly precipitation and temperature in various climate environments. Remediat. J. 99–108.
Worthy, W., Clarke, J.H., Abkowitz, M.D., 2013b. Surfactant-oxidation co-application for soil and groundwater remediation. Remediat. J. 26 (2), 101–108.
Worthy, W., Abkowitz, M.D., Clarke, J.H., 2015. A systematic approach to the evaluation of rcra disposal facilities under future climate-induced events. Remediat. J. 71–81.
Zachara, J.M., Long, P.E., Bargar, J., Davis, J.A., Fox, P., Fredrickson, J.K., Freshley, M.D., Konopka, A.E., Liu, C., McKinley, J.P., Rockhold, M.L., Williams, K.H., Yabusaki, S.B., 2013. Persistence of uranium groundwater plumes: contrasting mechanisms at two DOE sites in the groundwater-river interaction zone. J. Contam. Hydrol. 147, 45–72.